Geodesy and Geodynamics 11 (2020) 426–441

Contents lists available at ScienceDirect

Geodesy and Geodynamics

journal homepage: http://www.keaipublishing.com/geog

Diurnal variation of precipitable water vapor over Central and South America

Amalia Meza [a, b, *], Luciano Mendoza [a, b], María Paula Natali [a, b], Clara Bianchi [a, b], Laura Fernández [a, b]

[a] Laboratorio de Meteorología espacial, Atmósfera terrestre, Geodesia, Geodinámica, diseño de Instrumentaly Astrometría (MAGGIA), Facultad de Ciencias Astronómicasy Geofísicas (FCAG), Universidad Nacional de La Plata (UNLP), Paseo del Bosque s/n, B1900FWA, La Plata (UNLP), Paseo del Bosque s/n, B1900FWA, La Plata, Argentina

[b] Consejo Nacional de Investigación Científicay Técnica, Godoy Cruz 2290, C1425FQB, Buenos Aires, Argentina

ARTICLE INFO

Article history:
Received 8 January 2020
Accepted 22 April 2020
Available online 10 September 2020

Keywords:
Precipitable water vapor (PWV)
Global navigation satellite systems (GNSS)
Köppen and Geiger climate type classification (K-G)
Surface temperature
Principal component analysis (PCA)

ABSTRACT

Annual and seasonal diurnal precipitable water vapor (PWV) variations over Central and South America are analyzed for the period 2007–2013. PWV values were obtained from Global Navigation Satellite Systems (GNSS) observations of sixty-nine GNSS tracking stations. Histograms by climate categories show that PWV values for temperate, polar and cold dry climate have a positive skewed distribution and for tropical climates (except for monsoon subtype) show a negative skewed distribution.

The diurnal PWV and surface temperatures (T) anomaly datasets are analyzed by using principal components analysis (PCA). The first two modes represent more than 90% of the PWV variability. The first PCA mode of PWV variability shows a maximum amplitude value in the late afternoon few hours later than the respective values for surface temperature (T), therefore the temperature and the surface conditions (to yield evaporation) could be the main agents producing this variability; PWV variability in inland stations are mainly represented by this mode. The second mode of PWV variability shows a maximum amplitude at midnight, a possible explanation of this behavior is the effect of the sea/valley breeze. The coastal and valley stations are affected by this mode in most cases. Finally, the "undefined" stations, surrounded by several water bodies, are mainly affected by the second mode with negative eigenvectors. In the seasonal analysis, both the undefined and valley stations constitute the main cases that show a sea or valley breeze only during some seasons, while the rest of the year they present a behavior according to their temperature and the surface conditions. As a result, the PCA proves to be a useful numerical tool to represent the main sub-daily PWV variabilities.

1. Introduction

The Sun's energy drives the Earth's climate system, and the systematic differential heating of the world on different time scales influences weather and climate. The diurnal variation is a fundamental cycle, and a lot of atmospheric variables show characteristic day–night patterns. Regional diurnal variations are governed by the global pattern, but they are modulated by local features such as orography and land–sea interactions as well as transient events such as the passage of weather systems [1]. These complexities present challenges for quantification of the diurnal variabilities of atmospheric variables. Water vapor is one of the most important constituents of the Earth's atmosphere and contributes, on average, to about 60% of the greenhouse effect [2]. It also plays a crucial role in many other atmospheric processes. Typically, this gas makes up less than 1% of the atmosphere, but under very warm and moist conditions it can reach almost 4%.

The diurnal variation of the atmospheric water vapor affects surface and atmospheric long-wave radiation and atmospheric absorption of solar radiation (and thus, the surface temperature).

* Corresponding author. Laboratorio de Meteorología espacial, Atmósfera terrestre, Geodesia, Geodinámica, diseño de Instrumentaly Astrometría MAGGIA, Facultad de Ciencias Astronómicasy Geofísicas (FCAG), Universidad Nacional de La Plata (UNLP), Paseo del Bosque s/n, B1900FWA, La Plata, Argentina.
E-mail address: ameza@fcaglp.unlp.edu.ar (A. Meza).

Peer review under responsibility of Institute of Seismology, China Earthquake Administration.

Production and Hosting by Elsevier on behalf of KeAi

https://doi.org/10.1016/j.geog.2020.04.005

Diurnal variation of water vapor is also related to the diurnal variations of the moist convection, precipitation, and surface evapotranspiration [3–5].

Conventional techniques, such as upper air observations (radiosondes) and radiometer measurements, are not well suited to provide data with the required sampling, given the high spatial and temporal variability of precipitable water vapor (PWV). Accurate PWV measurements derived from Global Navigation Satellite Systems (GNSS) can provide valuable information about the water vapor content with much better spatial and temporal resolutions than conventional techniques [6–9]. The high quality and long-term stability of the GNSS estimates even make the use of these data possible in weather studies [10–12]. At present, the use of GNSS observations for PWV monitoring constitutes a widely employed and well tested technique. PWV estimates derived from GNSS, radiometer and upper air observations agree within 1.5 km/m^2 [6,13].

Hence, some authors have analyzed the diurnal cycle of water vapor over different regions and counties using GNSS observations. Dai et al. [5] studied the diurnal variation of precipitable water vapor over different regions of United States utilizing data from about fifty ground-based GPS stations. Radharkrishna et al. [14] used the North American Regional Reanalysis data and focused on the diurnal cycle, and they found the PWV peaks at late afternoon over Great Plain and at late night over Rockies. Their studies are mainly focused on the central United States, where they found a good agreement between the mean diurnal variations of PWV derived from the Global Positioning System (GPS) data, and sounding and microwave radiometer. The diurnal cycle which is the main component of the sub-daily variance, has an amplitude of about 1–2 mm in summer and lower in other seasons; whereas the PWV peaks are found around noon in winter and from mid-afternoon to mid-night in summer. Ortiz de Galisteo et al. [15] studied the annual and seasonal diurnal cycles of PWV over Spain. They found that the winter cycle is quite similar at all locations, while the summer one is not. Jakobson et al. [16] analyzed the PWV diurnal variability over the Baltic region and it shows a diurnal sinusoidal pattern with a maximum value in the afternoon for spring and summer. Kalinnikov and Khutorova [17] described diurnal and semidiurnal variations in PWV over the Volga-Ural region in Russia. They found that for most stations the maximum of diurnal harmonic winter and summer occurs within the period interval 14:00 to 17:00. Li et al. [18] analyzed the PWV diurnal cycle during calm summer days over central Japan and their results suggested that the diurnal variation of PWV is strongly affected by the local thermal circulations generated by the topography around the stations.

Here we study the mean diurnal variations in atmospheric PWV. This parameter is an important variable for improving our understanding of many atmospheric processes, particularly in the Tropics, as it has a tight relationship with convective processes and precipitation [19,20].

In addition, all the studies indicate that there are strong dependencies of the PWV diurnal cycle with the latitude dependence of the incoming solar radiation (i.e. seasons) and also with the topography where the GNSS stations are located, i.e. the proximity to a lake or an ocean coast, a valley, above a mountain or an island. Our work is focused on the characterization of the PWV obtained from GNSS (PWV_GNSS) diurnal variation over Central and South America by the application of principal component analysis (PCA). This work is an important contribution to study the PWV characterization and diurnal variation in this part of the planet. On one hand, there are only few works related to this topic and they are just focused on special regions (e.g. reference [21] showed the PWV diurnal variation in the Amazon area). On the other hand, the PCA technique proposed in our study is frequently used in the atmospheric sciences but not in PWV. Based on orthogonal decomposition of the data itself without forcing diurnal and semidiurnal components as in Fourier analysis, this technique becomes another way to analyze the PWV diurnal variation. Considering the Clausius–Clapeyron's equation, the higher the temperature the more PWV can be contained by the atmosphere before condensation takes place and this is the classical explanation of the main factor that produces the diurnal cycle of PWV. Therefore, the temperature should perhaps be the most important factor of the diurnal PWV variation. And PCA will also be applied on surface temperature to improve the analysis. Section 2 describes the employed data and the methodology used to define the sample in the numerical procedure, and section 3 shows the results, including the histograms by climate categories of the daily PWV values for all GNSS stations. Finally, the discussions and conclusions are presented in section 4.

2. Data and methodology

PWV values estimated over 69 GNSS stations located in Central and South America were employed (Fig. 1) with a sampling rate of 30 min for a period of about 5 years. These data are openly accessible, and detailed information about its computation and validation with upper air observations (radio sounding) can be found in reference [9].

Atmospheric surface temperature datasets provided by the University of Wyoming (UW, global surface observations available at http://weather.uwyo.edu/) and by the National Oceanic and Atmospheric Administration (NOAA, ISD-lite products available at ftp://ftp.ncdc.noaa.gov/pub/data/noaa/isd-lite/) were also employed in our analysis.

Firstly, both the PWV and surface Temperature (T) datasets were converted into diurnal anomalies by removing the corresponding daily means ΔPWV_{ijk} and ΔT_{ijk} are the diurnal anomaly, where i is each GNSS station, j is each one of the 48 values observed within each day and k is each day of the entire period. Then, the diurnal anomalies are averaged over the entire period. Therefore, the mean contribution to the PWV due to long-term systematic effects (i.e. longer than one day) were removed. Systematic errors with time scales close to a day, such as effects of tidal and ocean loading, are reduced when averages are built up using several years of data. Consequently, only the contribution of the terms that produce the small and regular diurnal change remains, and the regular diurnal variation of PWV can be studied [16].

2.1. Spatial and sub-hourly variability analysis

Here the diurnal anomalies are averaged over the corresponding time span, in order to obtain spatial (i.e. station position dependent) mean diurnal anomalies

$$\overline{\Delta PWV}_{ij} = \frac{1}{N}\sum_{k=1}^{N} \Delta PWV_{ijk} \quad (1)$$

where i represents the GNSS station, j indicates time (i.e. one value every half an hour), k and N represent each day and the total number of days for the respective time span, respectively. The same procedure is applied to the time series of surface temperature, in order to obtain mean values of the anomalies every 30 min $\overline{\Delta T}_{ij}$.

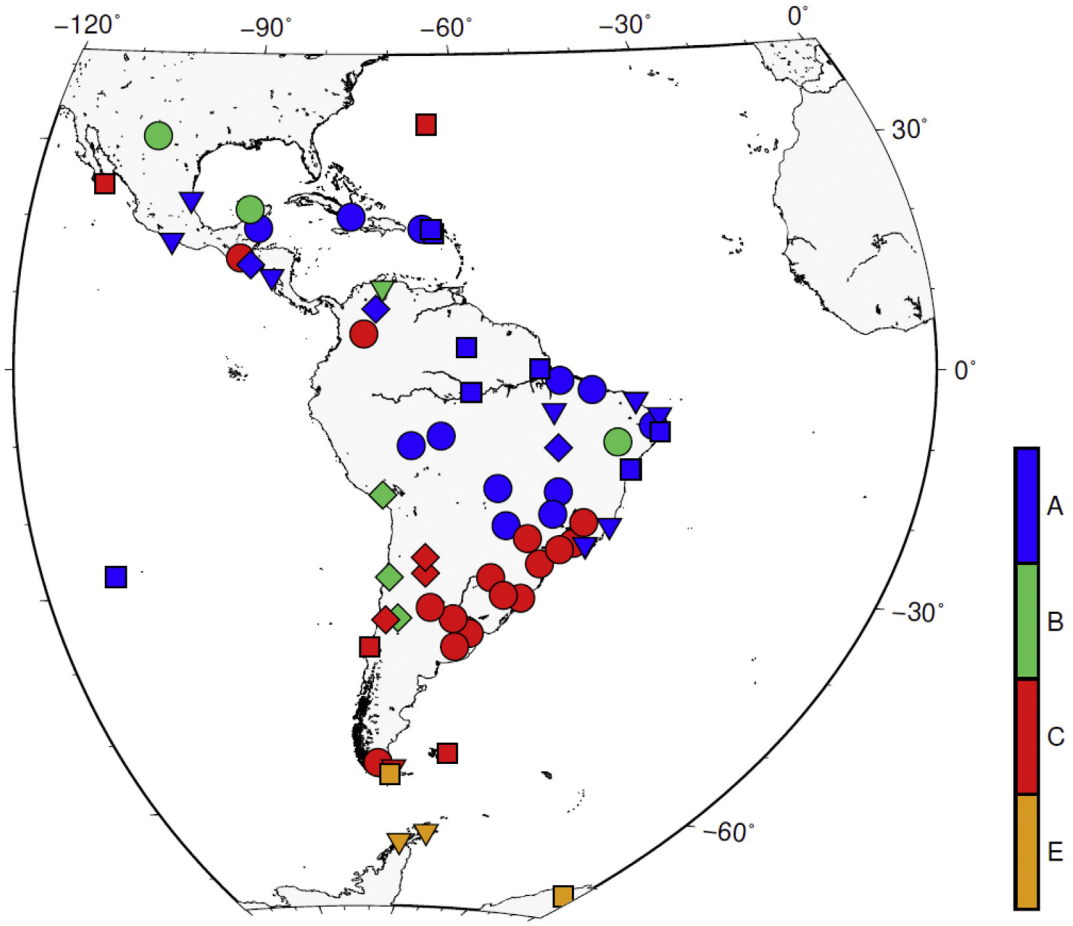

Fig. 1. Distributions of GNSS stations. The stations are defined by climate type and topography. The triangle, rhombus and circle represent coast (land at less than 5 km far from a clear body of water i.e. sea/lake), valley (surrounded by mountains) and inland (surrounded by regular surface) stations, respectively; the square represents the station without a clear topography classification (i.e.surrounded by different bodies of water) (see Table 1). The climate type classification scheme assigns four broad climatic zones: the equatorial zone (A, blue), the arid zone (B, green), the warm temperate zone (C, red), and the polar zone (E, orange).

2.2. PCA application

PCA is a powerful technique for multivariate time series analysis. This technique assumes that a set of observed variables are correlated through first order linear dependencies and provides a way to build a new set of uncorrelated variables that, in turn, allow the reconstruction of the complete observed dataset. This feature is a strong motivation to use PCA because that a small set of uncorrelated variables which completely represents a dataset can also be related to a combination of a small number of independent physical phenomena.

The set of uncorrelated variables provided by PCA constitutes an orthonormal base of minimum dimension. The aspect of these eigenvectors is solely determined by the observation set. Thus, they may not necessarily be described by means of simple mathematical expressions. This is the reason why PCA is a well suited technique for multivariate datasets analysis, when the underlying phenomena are known to not be the superposition of well-defined components. Otherwise, more adequate techniques can be applied (e.g., Fourier analysis).

We just present a brief description of the technique above and further details about algebraic foundations of PCA can be found in references [22,23].

Next, the procedure used to implement PCA method on PWV observations is delineated.

$\boldsymbol{V}$ is the matrix that contains the spatial mean diurnal anomalies of PWV.

$$\boldsymbol{V} = \begin{pmatrix} v_{1,1} & \cdots & v_{1,n_{\text{epoch}}} \\ \vdots & \ddots & \vdots \\ v_{n_{\text{sta}},1} & \cdots & v_{n_{\text{sta}},n_{\text{epoch}}} \end{pmatrix} = \begin{pmatrix} \overline{\Delta\text{PWV}}_{1,0:00} & \cdots & \overline{\Delta\text{PWV}}_{1,23:30} \\ \vdots & \ddots & \vdots \\ \overline{\Delta\text{PWV}}_{n_{\text{sta}},0:00} & \cdots & \overline{\Delta\text{PWV}}_{n_{\text{sta}},23:30} \end{pmatrix} \left(n_{\text{sta}} \times n_{\text{epoch}}\right) \quad (2)$$

where $n_{\text{sta}} = 69$ and $n_{\text{epoch}} = 48$ (n_{sta} is the number of station and n_{epoch} refers to the 30 min values along the day).

Firstly, from $\boldsymbol{V}$, we can compute the per-row averages (i.e. time averages) in order to populate the following mean array

$$\overline{\boldsymbol{V}} = \begin{pmatrix} \overline{v}_1 & \cdots & \overline{v}_1 \\ \vdots & \ddots & \vdots \\ \overline{v}_{n_{\text{sta}}} & \cdots & \overline{v}_{n_{\text{sta}}} \end{pmatrix} \left(n_{\text{sta}} \times n_{\text{epoch}}\right) \quad (3)$$

Then, from $\boldsymbol{V}$, we subtract to each row its own time average in order to obtain per-row-centered (i.e. zero mean) datasets.

$$\boldsymbol{V}' = \boldsymbol{V} - \overline{\boldsymbol{V}}\left(n_{\text{sta}} \times n_{\text{epoch}}\right) \quad (4)$$

In the second step, we define the scatter array $\boldsymbol{S}$ as:

$$\boldsymbol{S} = \boldsymbol{V'}^{\mathrm{T}}\boldsymbol{V'}\left(n_{\mathrm{sta}} \times n_{\mathrm{epoch}}\right) \tag{5}$$

As $\boldsymbol{S}$ is a square array, it has a set of orthonormal eigenvectors. This set can be used as a new base to represent the scatter array and to subsequently construct the principal components array $\boldsymbol{A}$.

$$\boldsymbol{A} = \boldsymbol{V'}^{\mathrm{T}}\boldsymbol{E}\left(n_{\mathrm{sta}} \times n_{\mathrm{epoch}}\right) \tag{6}$$

where the columns of $\boldsymbol{E}$ are the eigenvectors of $\boldsymbol{S}$. Then using the property $\boldsymbol{E}\boldsymbol{E}^{\mathrm{T}} = \boldsymbol{I}$, the original zero mean datasets can be expressed as:

$$\boldsymbol{A}\boldsymbol{E}^{\mathrm{T}} = \boldsymbol{V'}^{\mathrm{T}}\left(n_{\mathrm{sta}} \times n_{\mathrm{epoch}}\right) \tag{7}$$

Coming back to our original dataset, Eq. (2) can be rewritten by using PCA as:

$$\boldsymbol{V}^{\mathrm{T}} = \overline{\boldsymbol{V}}^{\mathrm{T}} + \boldsymbol{A}\boldsymbol{E}^{\mathrm{T}}\left(n_{\mathrm{epoch}} \times n_{\mathrm{sta}}\right) \tag{8}$$

The eigenvectors (i.e., columns, $\boldsymbol{e_1}$ is the column 1 and so on.) in $\boldsymbol{E}$ represent the spatial structure of $\overline{\Delta \mathrm{PWV}}_{ij}$variability, while the coefficients (i.e., columns, a_1 is the column 1 and so on.) of $\boldsymbol{A}$ which are called principal components characterize the temporal information of $\overline{\Delta \mathrm{PWV}}_{ij}$variability. Thus, we call "modes" of variability to each pair eigenvectors and principal components. And these "modes" are sorted according to decreasing corresponding eigenvalues magnitude (according to its significance). In practice, only a few of these modes are enough to generate most of the original observed signals. Of course, the same PCA analysis was performed on the temperature mean diurnal anomalies.

3. Results

3.1. Notes on the climate type classification and temperature

In this study, in order to better characterize the PWV observations, all GNSS stations are arranged according to the Köppen and Geiger (K-G) climate type classification [24]. The K-G system, which is constructed on the basis of five vegetation groups, is based on a large of global datasets of long-term monthly temperature and precipitation time series. Peel et al. [24] have made their global climate map available as a supplementary material. According to their predominant vegetation, this classification scheme allocates five broad climate zones: the equatorial zone (A), the arid zone (B), the warm temperate zone (C), the snow zone (D) and the polar zone (E) [25]. Moreover, the climate subtypes are defined with additional two letters which are related to the precipitation and the air temperature [24].

Hence, we were able to compute climate type-specific histograms of the daily PWV observations with the corresponding GNSS stations (Fig. 2).

For stations with tropical climate (type A), the PWV values range between 10 kg/m^2 and 65 kg/m^2 (Fig. 2a). Lower values are typical for tropical stations at higher altitudes. For stations with subtype monsoon (Am), the PWV values have the maximum frequency at about 54 kg/m^2 while for dry summer (As) and dry winter (Aw) subtypes, their maximum frequencies are at about 34 kg/m^2 and 40 kg/m^2, respectively; for rainforest (Af) subtype, the maximum frequency in PWV values is similar to dry winter subtype (Fig. 2b). Except for dry summer subtype, Fig. 2b shows a negatively skewed distribution for all cases.

For stations with dry climate (type B), the analyses show a remarkable different behavior among the subtypes (Fig. 2c); the stations with hot steppe climate (BSh) show PWV values ranging between 12 kg/m^2 and 65 kg/m^2 with the maximum frequency at about 35 kg/m^2, while those stations with cold steppe climate (BSk) or cold desert (BWk) show PWV values ranging between 2 kg/m^2 and 30 kg/m^2 with the maximum frequency at about 10 kg/m^2 (Fig. 2d). For cold cases, Fig. 2d shows a positive skewed distribution, while for hot ones it shows a negatively skewed distribution (or even a bimodal distribution).

For those stations with temperate climate, the PWV values range between 2 kg/m^{2}and 55 kg/m^2 (Fig. 2e). The stations with humid tropical climate subtype (Cfa) and temperate oceanic climate subtype (Cfb) show the maximum PWV value around 15 kg/m^2. The stations with subpolar oceanic climate subtype (Cfc) show PWV values ranging between 2 kg/m^{-2} and 20 kg/m^2 and the maximum value is around 10 kg/m^2. The stations with warm-summer mediterranean climate subtype (Csb) show PWV values ranging between 2 kg/m^2 and 35 kg/m^2 and the maximum frequency is around 14 kg/m^2. The stations with monsoon-influenced humid subtropical climate subtype (Cwa) show the PWV values ranging between 2 kg/m^2 and 50 kg/m^2 with the maximum frequency at about 20 kg/m^2 (Fig. 2f). The stations with monsoon-influenced temperate oceanic climate subtype (Cwb) show the PWV values ranging between 2 kg/m^2 and 60 kg/m^2 with the maximum frequency at about 15 kg/m^2 (Fig. 2f). Fig. 2f shows a positively skewed distribution for all cases.

For stations with polar climate (polar tundra (ET) and polar frost (EF) were grouped in type E), the PWV values range between 2 kg/m^2 and 20 kg/m^2 with the maximum frequency at about 5 kg/m^2 and it shows a positively skewed distribution in Fig. 2g.

From the above, Fig. 2 represents that there are some discrepancies in the PWV histograms which are generated considering stations that belong to the same climate type. Therefore, we build up histograms for each GNSS station in order to improve our analysis.

Fig. 3, showing the histograms of some selected stations, evidences the relationship between their geographic latitudes and heights, and PWV distribution. In the same graph, the climate type is also included. These histograms show that the mean PWV value is strongly correlated with the latitudes for stations at low altitudes. At equatorial latitude the mean PWV value is larger than that at mid-latitude and the histograms mostly represent a lognormal frequency shape, except for equatorial stations (which belong to Af, Am and BSh climates subtypes) that behave similarly to a reverse-lognormal distribution, only in few cases the histograms show a clear bimodal distribution (e.g. BRAZ station).

The mean PWV values for stations at higher altitudes (e.g. larger than 200 m) are smaller than the mean PWV values for stations at similar latitudes, but at lower altitudes, e.g. PBCG and POVE stations or PEPE and MARA stations (Fig. 3). The stations at higher altitudes show lognormal and bimodal frequency distributions.

3.2. Spatial and sub-hourly variability analysis

In this section the annual and seasonal diurnal variations of PWV and T are analyzed. Firstly, the described PCA analysis was applied to the mean diurnal anomalies in both PWV and T, over the complete data time span (i.e., more than five years). Secondly, very same methodology was applied to the data subsets, spanning the

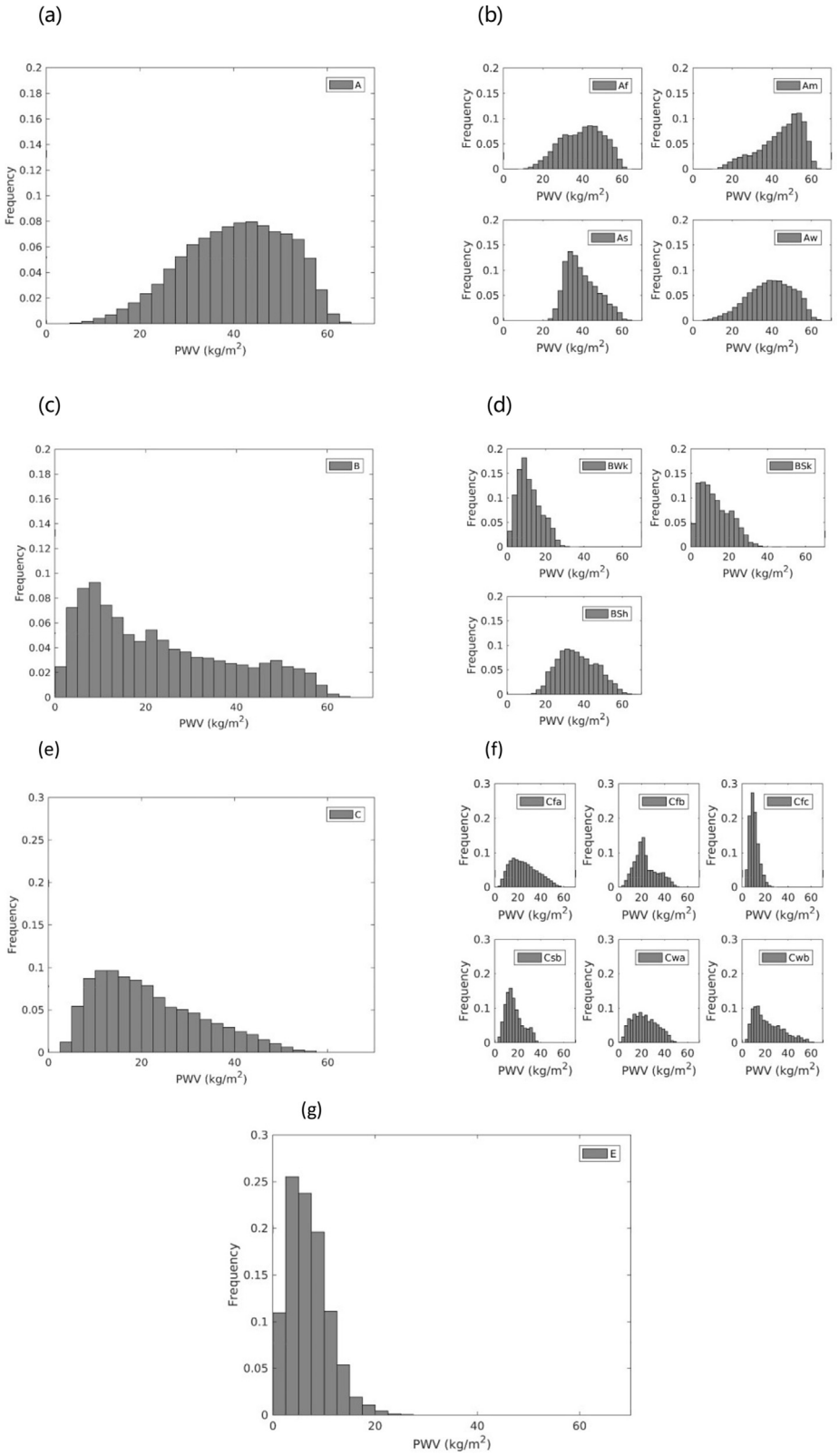

Fig. 2. The histograms by K-G climate categories of the daily PWV values. Left column shows the frequency versus daily mean PWV in kg/m^2 according to the different climate types. Right column shows the behavior of frequency versus daily mean PWV in kg/m^2 for the respective climate subtypes.

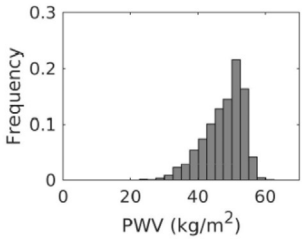	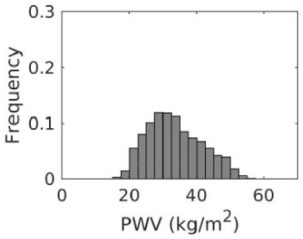	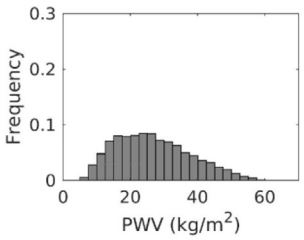
Name: NAUS Mean PWV: 47.5 kg/m^{22} Latitude: -3.02° Height: 93 m K-G: Am	Name: PEPE Mean PWV: 33.6 kg/m^2 Latitude: -9.38° Height: 369 m K-G: BSh	Name: POAL Mean PWV: 26.9 kg/m^2 Latitude: -30° Height: 76.7 m K-G: Cfa
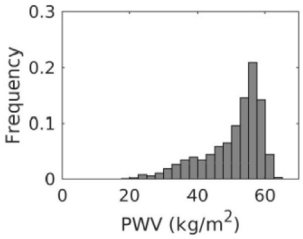	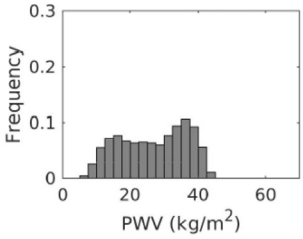	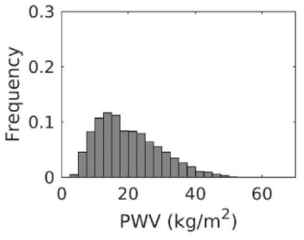
Name: POVE Mean PWV: 50,4 kg/m^2 Latitude: -8,70° Height: 119 m K-G: Am	Name: BRAZ Mean PWV: 26.7 kg/m^2 Latitude: -15.9° Height: 1106 m K-G: Aw	Name: IGM1 Mean PWV: 20.1 kg/m^2 Latitude: -34,5° Height: 50.7 m K-G: Cfa
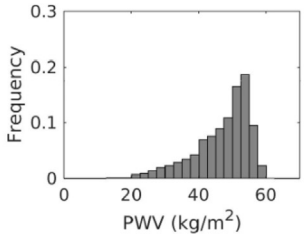	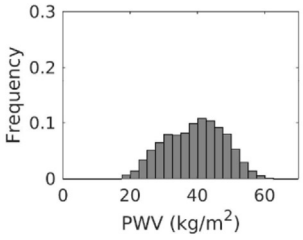	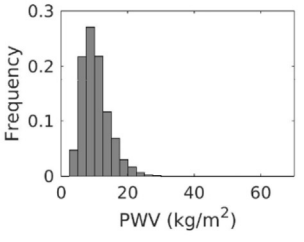
Name: RIOB Mean PWV: 46,9 kg/m^2 Latitude: -9,97° Height: 172 m K-G: Af	Name:BYSP Mean PWV: 39.20 kg/m^{2}Latitude: 18.40° Height: 49.2 m K-G: Af	Name: PARC Mean PWV: 10.3 kg/m^{2}Latitude: -53.1° Height: 22.3 m K-G:Cfc
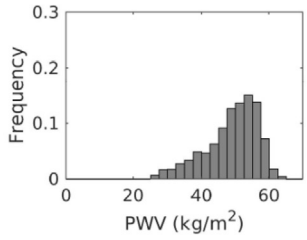	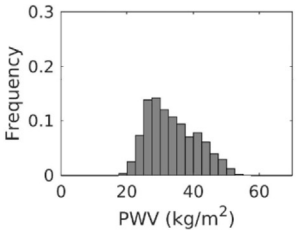	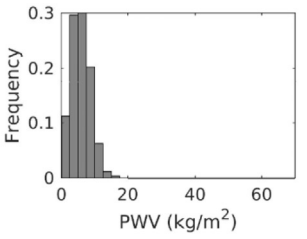
Name :MARA Mean PWV: 48.9 kg/m^2 Latitude: -10.67° Height: 28 m K-G: BSh	Name: PBCG Mean PWV: 33,6 kg/m^2 Latitude: -7.21° Height: 534 m K-G: Aw	Name: OHI2 Mean PWV: 5.9 kg/m^2 Latitude: -63.3° Height: 32.5 m K-G: EF

Fig. 3. The histograms for selected GNSS stations (frequency versus daily mean PWV in kg/m^2).

very same period, corresponding to the four seasons: December, January and February (DJF); March, April and May (MAM); June, July and August (JJA) and September, October and November (SON). Moreover, before both analyses, the stations were divided into four classes: stations surrounded by land with smooth topography (the "inland" stations); stations located less than 5 km from a body of water (sea, lake or lagoon, the "coastal" stations); stations surrounded by mountains (the "valley" stations) and stations that do not conform to any of the previous three classes (the "undefined" stations). A list of stations which are classified according to their locations is given in Table 1, whereas their spatial distributions and corresponding climate types are shown in Fig. 1.

3.2.1. Annual analysis

In this case we found that the first two modes explain up to 97% of the total variance of the PWV (Table 2), whereas for the temperature T the same percentage can be achieved by the first mode alone. Fig. 4a and c show the first mode of PWV (70% of the variability). Its principal component (section 2.2, Eq. (6)) shows a diurnal variability (Fig. 4c, dotted black line), with the maximum value at 19:00 Local Time (LT) and the minimum value at 9:00 LT (Fig. 4c, dotted gray line). The increase, from minimum to maximum, spans approximately 10 h, while the subsequent decrease is slower. These maximum and minimum values occur about 4 h and 3 h later respectively than the corresponding extrema in the principal component of T (Fig. 5b). Fig. 4a shows the first eigenvector, when it has positive values, the diurnal PWV variability has the maximum at 19:00 LT; while it has negative values, the diurnal PWV variability has the maximum value during morning hours. Not all stations present positive eigenvectors of PWV (Fig. 4a), which indicates that there are some stations in counter phase with respect to the principal component pattern described before.

A 27% of the PWV variability is represented by the second mode (Fig. 4b and c), and its principal component also shows a diurnal variability (Fig. 4c). In this case, the maximum value occurs at midnight and the minimum value appears at 15:00 LT, almost in coincidence with the maximum value of the first principal component in T.

In essence, the annual analysis of the PCA shows a common pattern of diurnal variation of the PWV. Most stations show the maximum and minimum values a few hours after the respective extremes in T (Fig. 5). However, there are a significant number of stations that clearly do not share this behavior. Given the varied topographies of the study regions (e.g., the Andes cordillera, the Amazon rain-forest, great valley and steppes), these different variabilities in PWV are to be expected.

According to the Clausisus–Clapeyron equation, the logarithm of the vapor pressure will increase as the temperature of the system increases, before the condensation takes place. Therefore, the classic idea is that the diurnal warming drives evaporation/evapotranspiration and increases the PWV, while cooling causes its decrease at night. Stations in Fig. 4a show positive eigenvectors of the first mode, which are multiplied by the respective principal component (Fig. 4c), represent a PWV variability with the minimum and maximum values at 9:00 LT and at 19:00 LT, respectively. They take place a few hours after the extreme values of the first PCA mode of the surface temperature (Fig. 5) which are about 6:00 LT and 15:00 LT, respectively.

Fig. 6 represents the reconstruction of the annual diurnal PWV variability based on the first two PCA modes for selected: inland (a), coastal or valley (b) and "undefined" (c) stations. The inland stations have a diurnal PWV variability in agreement with the Clausius–Clapeyron equation (Fig. 6a). In this case the first eigenvector has positive values and the second eigenvector has values much smaller than the first one, or it has negative values with similar magnitude to the first one. The maximum and minimum diurnal PWV variability are reached between 17:00 LT and 19:00 LT, and between 7:00 LT and 9:00 LT respectively, and its maximum amplitude reaches a value up to 3 kg/m^2. These results could be produced by the temperature and the surface conditions (to yield evaporation).

The last two cases (b and c) don't satisfy the previous behavior, and that is strongly related to the idea that the diurnal cycle of temperature is not the only agent that explains the diurnal PWV variability. The maximum PWV variability is around midnight as was highlighted by other authors [5,15,18,26]. This behavior is related to the advection of humid or dry air masses; the local geographical conditions can be responsible for the circulation patterns that occur almost every day such as land and sea breeze or mountain and valley breeze. The differential warming between land and a large body of water or mountain and valley, carry moisture onshore/upslope at daytime while during the night this circulation is reversed (offshore/downslope) due to the faster cooling of the land/mountain surfaces. Also, in some cases, these influences are dependent on the time of the year due to the annual variability of the circulation pattern [26].

For the last case (c), stations classified as "undefined" are surrounded by several water bodies. .For the last case (c), stations classified as "undefined" are surrounded by several water bodies. Their first eigenvector is negative and the second eigenvector can be either negative or very small positive values. Both the maximum PWV and T variabilities happen almost simultaneously (around midday). One result of the previous PWV variability could be produced when the morning sea breeze is replaced by much dryer air if the wind changes direction. Taking into account the location of these stations, the sea breeze produced by one of the water bodies close to the station begins to weaken in the late evening while the other water body produce a wind transport moisture and consequently the PWV increases (even when surface temperature is decreasing) [15].

Table 2 summarizes the percentage of variability explained by each principal component, the type of station, and some possible associated physical phenomena.

3.2.2. Seasonal analysis

Finally, the seasonal diurnal PWV variability is analyzed. Therefore, PCA is applied to the seasonal mean PWV and T diurnal anomalies (section 2). The first two modes explain up to 95% of the total variance of the PWV for all seasons, while for the temperature T the same percentage is represented by the first mode alone (These figures are not showed because they are very similar to Fig. 5.).

Figs. 7–10 show the eigenvalues and principal components. And they are similar to Fig. 4 but for each season.

For DJF, Fig. 7a and c show the first mode of the PWV variability (73% of the variability). Its principal component (section 2.2, Eq. (6)) shows a diurnal variability (Fig. 7c), with the maximum value at 18:30 LT and the minimum value at 9:00 LT. The 22% of the PWV variability is represented by the second mode (Fig. 7b and c), and its principal component shows a diurnal variability (Fig. 7c). In this case, the maximum value occurs at the midnight and the minimum value appears at 14:30 LT.

For MAM, Fig. 8a and c show the first mode of the PWV variability (69% of the variability). Its principal component (section 2.2, Eq. (6)) shows a diurnal variability (Fig. 8c), with the maximum

Table 1
Location and K-G climate classifications of the GNSS stations.

Name of GPS station	Longitude (°)	Latitude (°)	Height (m)	Climate type	Classification
BELE	−48.4626	−1.4088	9.1	Af	Inland
BYSP	−66.1612	18.4078	49.2	Af	Inland
CUCU	−72.4879	7.8985	311.2	Af	Valley
RIOB	−67.8028	−9.9655	172.6	Af	Inland
SAVO	−38.4323	−12.9392	76.3	Af	Undefined
SSA1	−38.5165	−12.9752	−2.1	Af	Undefined
ISPA	−109.3444	−27.1250	112.5	Af	Undefined
MAPA	−51.0973	0.0467	−4.2	Am	Undefined
NAUS	−60.0550	−3.0229	93.9	Am	Undefined
ONRJ	−43.2243	−22.8957	35.6	Am	Coast
POVE	−63.8963	−8.7093	119.6	Am	Inland
RIOD	−43.3063	−22.8178	8.6	Am	Coast
RECF	−34.9515	−8.0510	20.1	As	Undefined
RNNA	−35.2077	−5.8361	45.9	As	Coast
ACYA	−99.9030	16.8380	−4.9	Aw	Coast
BOAV	−60.7011	2.8452	69.5	Aw	Undefined
BRFT	−38.4255	−3.8774	21.7	Aw	Coast
CEEU	−38.4255	−3.8775	21.7	Aw	Coast
CEFE	−40.3195	−20.3108	14.3	Aw	Coast
CHET	−88.2992	18.4953	3.0	Aw	Inland
CRO1	−64.5843	17.7569	−32.0	Aw	Undefined
CUIB	−56.0699	−15.5553	237.5	Aw	Inland
MABA	−49.1223	−5.3624	79.8	Aw	Coast
MANA	−86.2490	12.1489	71.0	Aw	Coast
MSCG	−54.5407	−20.4409	676.5	Aw	Inland
PBCG	−35.9071	−7.2137	534.1	Aw	Inland
SALU	−44.2125	−2.5935	19.0	Aw	Inland
SCUB	−75.7623	20.0121	20.9	Aw	Inland
SSIA	−89.1166	13.6971	626.6	Aw	Valley
TAMP	−97.8640	22.2783	21.0	Aw	Coast
TOPL	−48.3307	−10.1711	256.5	Aw	Valley
VITH	−64.9692	18.3433	4.4	Aw	Undefined
BRAZ	−47.8779	−15.9475	1106.0	Aw	Inland
UBER	−48.3170	−18.8895	791.8	Aw	Inland
MARA	−71.6244	10.6740	28.4	BSh	Coast
MERI	−89.6203	20.9800	7.9	BSh	Inland
PEPE	−40.5061	−9.3844	369.1	BSh	Inland
MDO1	−104.0150	30.6805	2004.5	BSk	Inland
MZAC	−68.8756	−32.8952	859.9	BSk	Valley
AREQ	−71.4928	−16.4655	2488.9	BWk	Valley
COPO	−70.3382	−27.3845	479.1	BWk	Valley
BRMU	−64.6963	32.3704	−11.6	Cfa	Undefined
EBYP	−55.8922	−27.3689	139.8	Cfa	Inland
IGM1	−58.4393	−34.5722	50.7	Cfa	Inland
LPGS	−57.9323	−34.9067	29.9	Cfa	Inland
POAL	−51.1198	−30.0740	76.7	Cfa	Inland
PPTE	−51.4085	−22.1199	431.0	Cfa	Inland
SMAR	−53.7166	−29.7189	113.1	Cfa	Inland
TUCU	−65.2304	−26.8433	485.0	Cfa	Valley
UFPR	−49.2310	−25.4484	925.8	Cfa	Inland
UNRO	−60.6284	−32.9594	66.9	Cfa	Inland
AZUL	−59.8813	−36.7670	158.3	Cfb	Inland
BOGT	−74.0809	4.6401	2576.4	Cfb	Inland
CHPI	−44.9852	−22.6871	617.4	Cfb	Inland
POLI	−46.7303	−23.5556	730.6	Cfb	Inland
FALK	−57.8741	−51.6937	50.8	Cfc	Undefined
PARC	−70.8799	−53.1370	22.3	Cfc	Inland
RIO2	−67.7511	−53.7855	32.0	Cfc	Coast
CONZ	−73.0255	−36.8438	180.6	Csb	Undefined
GUAT	−90.5202	14.5904	1519.9	Csb	Inland
SANT	−70.6686	−33.1503	723.1	Csb	Valley
MGBH	−43.9249	−19.9419	974.8	Cwa	Inland
UCOR	−64.1935	−31.4350	462.8	Cwa	Inland
LPAZ	−110.3194	24.1388	−6.9	Cwb	Undefined
UNSA	−65.4076	−24.7275	1257.8	Cwb	Valley
OHI2	−57.9013	−63.3211	32.5	EF	Coast
PALM	−64.0511	−64.7751	31.1	EF	Coast
VESL	−2.8418	−71.6738	862.4	EF	Undefined
AUTF	−68.3036	−54.8395	71.9	ET	Undefined

Notes:K-G climate classification. A: tropical climate (f: rainforest, m: monsoon, s: dry summer,w: dry winter); B: dry climate (Wk: cold desert, Sh: hot steppe,Sk: cold steppe); C: temperate climate (fa: humid subtropical, fb: oceanic, fc: subpolar oceanic, wa: monsoon-influenced humid subtropical, wb: monsoon-influenced temperate oceanic,sb: warm-summer mediterranean) and E: polar (T: tundra,F: ice cap).

Table 2
Summary of the PCA results according to the types of stations.

Mode type	Percentage of the variability	Observation
First	70%	The eigenvector is positive and has a a lag-time of about 3–4 h respect to T variability, that is related to the solar heating. Inland stations which are the 45% of the stations are mainly affected by this mode.
Second	27%	When eigenvector is positive, it has a lag-time of 6–7 h respect to the first mode (and nearly out-of-phase with T variability). It shows the action of an agent that triggers an increase of the water vapor at the night hour. This behavior could be related to the advection of humid or dry air masses and the local geographical conditions can be responsible in circulation patterns such as land and sea breeze or mountain and valley breeze. The coastal and valley stations (which are 33% of the stations) are affected by this mode in most cases. When eigenvector is negative, the maximum PWV variability happens almost simultaneously with the maximum T variability. This situation occurs when the station is surrounded by several water bodies.One result of the previous PWV variability could be produced when the morning sea breeze is replaced by much dryer air if the wind changes direction. This kind of stations are classified as "undefined" (which are 15% of the stations).

value at 18:30 LT and the minimum value at 9:00 LT. The 26% of the PWV variability is represented by the second mode (Fig. 8b and c), and its principal component shows a diurnal variability (Fig. 8c). In this case, the maximum value occurs at midnight and the minimum value appears at 15:00 LT.

For JJA, Fig. 9a and c show the first mode of the PWV variability (67% of the variability). Its principal component (section 2.2, Eq. (6)) shows a diurnal variability (Fig. 9c), with the maximum value at 21:00 LT and the minimum value at 9:30 LT. The 28% of the PWV variability is represented by the second mode (Fig. 9b and c), and its

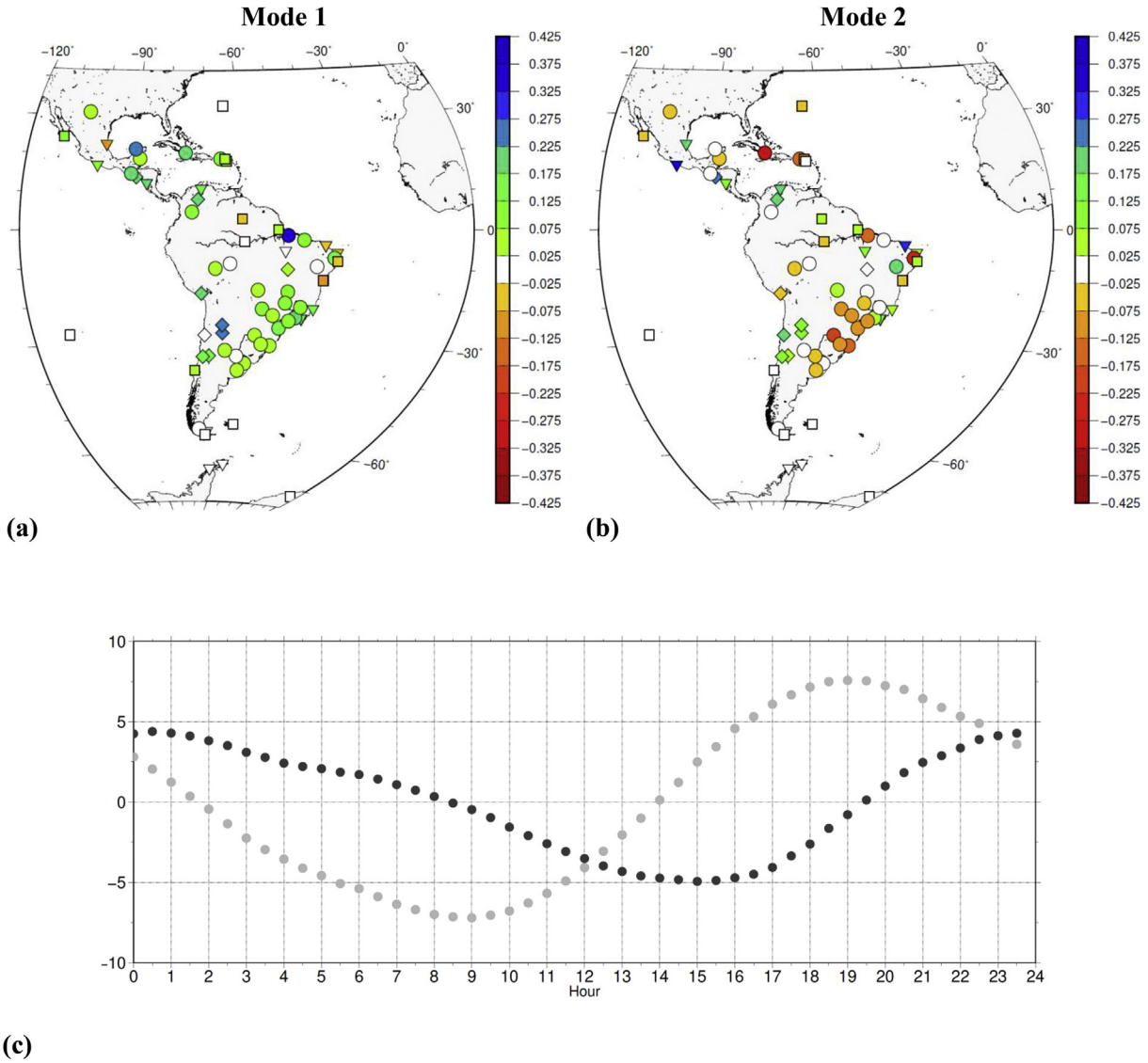

Fig. 4. PCA analysis for annual diurnal variability of PWV. (a) eigenvector of the first mode,$\boldsymbol{e_1}$; (b) eigenvector of the second mode, $\boldsymbol{e_2}$; (c) principal components of the first and second modes,a_1 (grey) and a_2 (black) respectively.

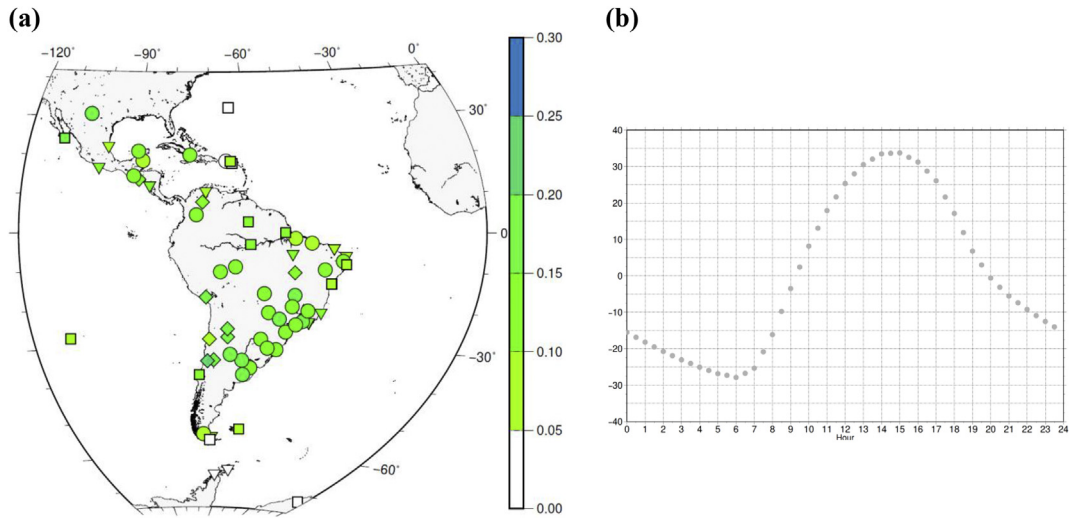

Fig. 5. Mode 1 of PCA analysis over the annual diurnal variability of temperature. (a) eigenvector of the first mode, $\boldsymbol{e_1}$; (b) principal component of the first mode, a_1.

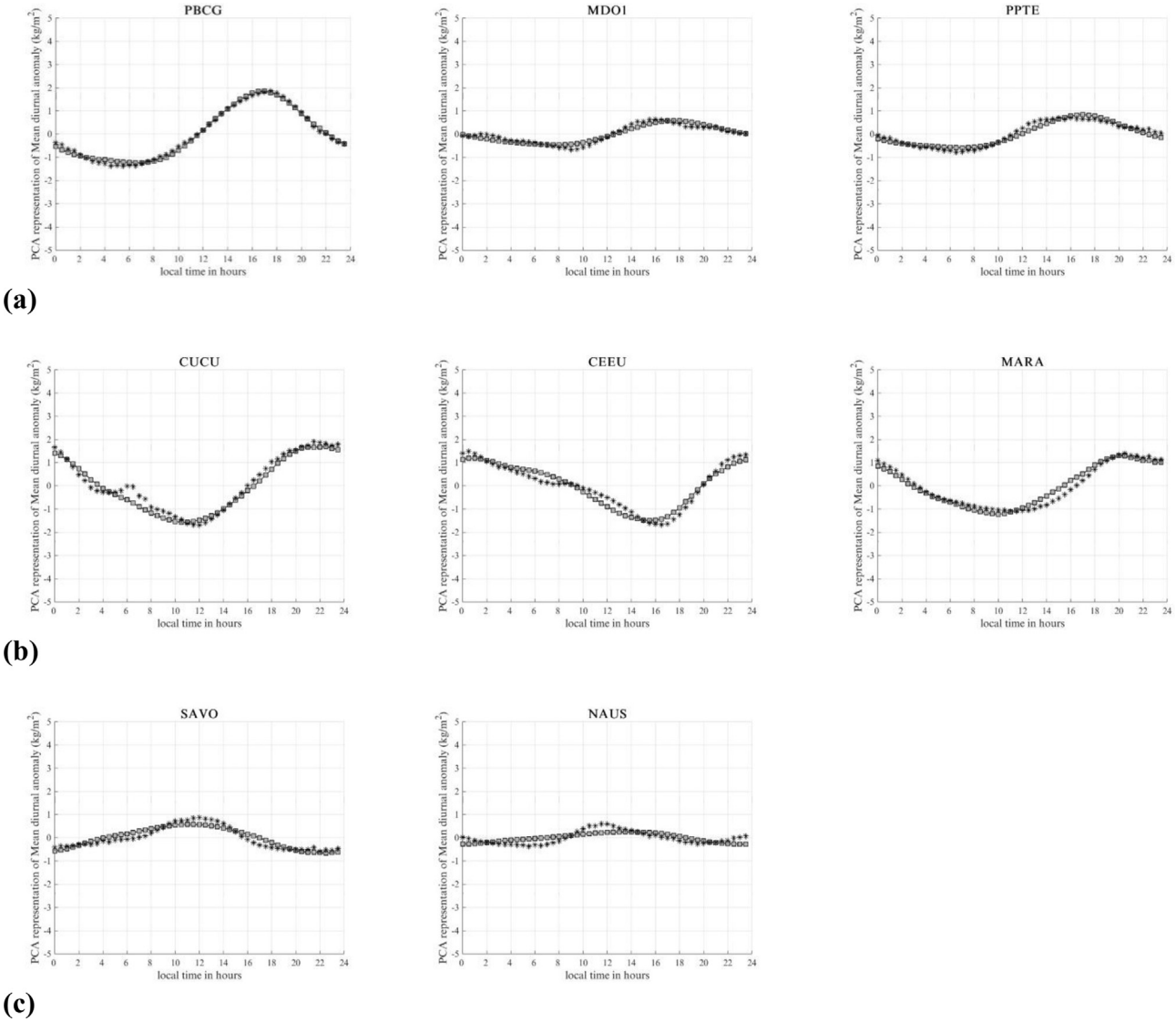

Fig. 6. PCA reconstruction of the annual diurnal PWV variability. Reconstruction of the annual diurnal variability of PWV using the first and second PCA modes (squares) and the original cycle (asterisk) for selected (a) inland, (b) coastal or valley, and (c) "undefined" stations.

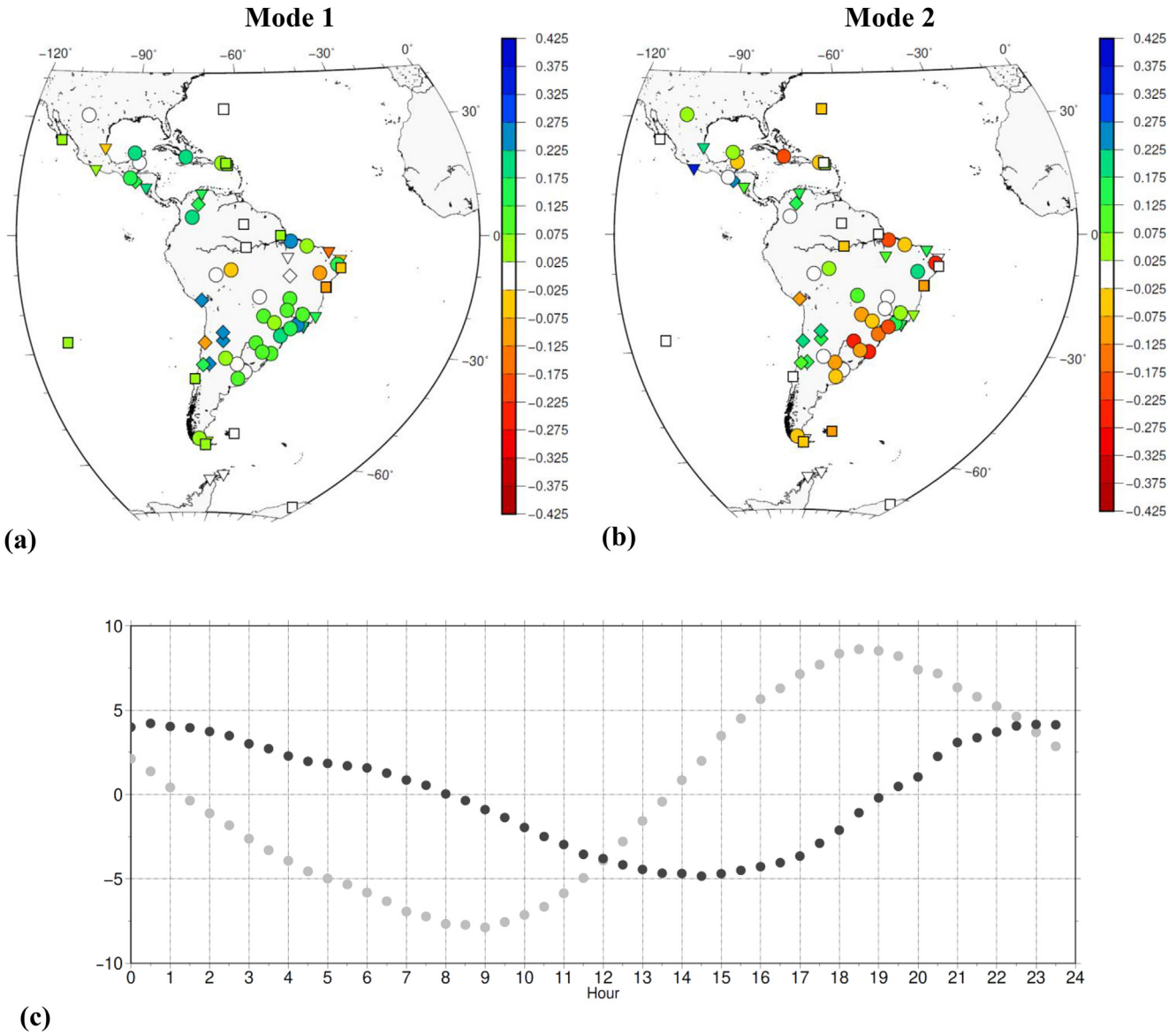

Fig. 7. PCA analysis for the DJF diurnal variability of PWV. (a) eigenvector of the first mode, $\boldsymbol{e}_1$; (b) eigenvector of the second mode,$\boldsymbol{e}_2$; (c) principal components of the first and second modes, a_1 (grey) and a_2 (black) respectively.

principal component shows a diurnal variability (Fig. 9c). In this case, the maximum value occurs at the midnight and the minimum value at 16:00. LT.

For SON, Fig. 10a and c exhibit the first mode of the PWV variability (64% of the variability). Its principal component (section 2.2, Eq. (6)) shows a diurnal variability (Fig. 10c), with the maximum value at 19:00 LT and the minimum value at 8:00. LT. The 31% of the PWV variability is represented by the second mode (Fig. 10b and c), and its principal component shows a diurnal variability (Fig. 10c). In this case, the maximum value occurs at the midnight and the minimum value at 15:00 LT.

In all cases the maximum and minimum values of the first principal component occur respectively at least 3.5 h and 2 h later than the corresponding extrema in the principal component of T, while the second principal component has the minimum value almost in coincidence with the maximum value of the first principal component in T.

For all inland stations located at mid-latitudes, as well for the most of the coastal and valley stations, the maximum amplitude of diurnal variability of PWV is found at local summer. For those stations located at low latitudes or close to the Equator, the maximum amplitude of diurnal variability of PWV is found during the equinoxes. In general, almost all stations (i.e. more than 80%) show a similar pattern of variability of the diurnal PWV anomaly in all seasons of the year. In these cases, the amplitude values can be different, and the times at which the extreme values are recorded only present differences lesser than one hour. However, around 27% of the total number of stations that were classified as valley and "undefined" show different diurnal variabilities of the PWV during the different seasons of the year. Examples of this behavior are MAPA (undefined) and AREQ (valley) (Fig. 11a). Moreover, there are some other particular stations (BELE and POVE stations, see Fig. 11b) with inland behavior but showing the maximum value of PWV diurnal variabilities at the night when a seasonal analysis is performed. BELE station shows the maximum values during the night in JJA while for the other seasons their behavior is similar to an inland station that is in agreement with the results obtained by Adams et al. [21]. And they found a diurnal cycle of sea-breeze convection for Belem (i.e. BELE station) to analyze PWV variability from May 25 to July 7, 2011.

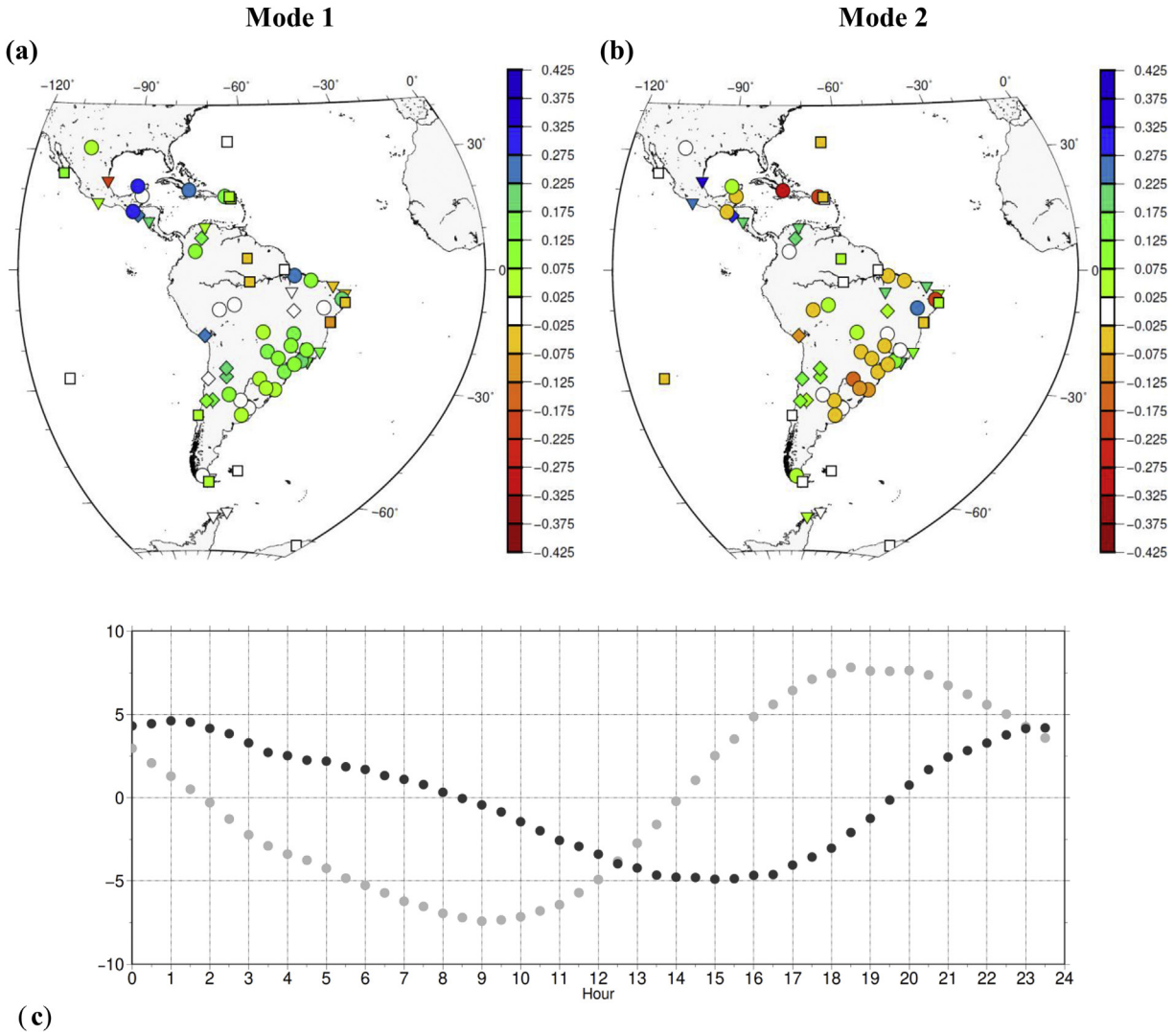

Fig. 8. PCA analysis for the MAM annual diurnal variability of PWV. (a) eigenvector of the first mode, $\boldsymbol{e_1}$; (b) eigenvector of the second mode, $\boldsymbol{e_2}$; (c) principal components of the first and second modes, a_1 (grey) and a_2 (black) respectively.

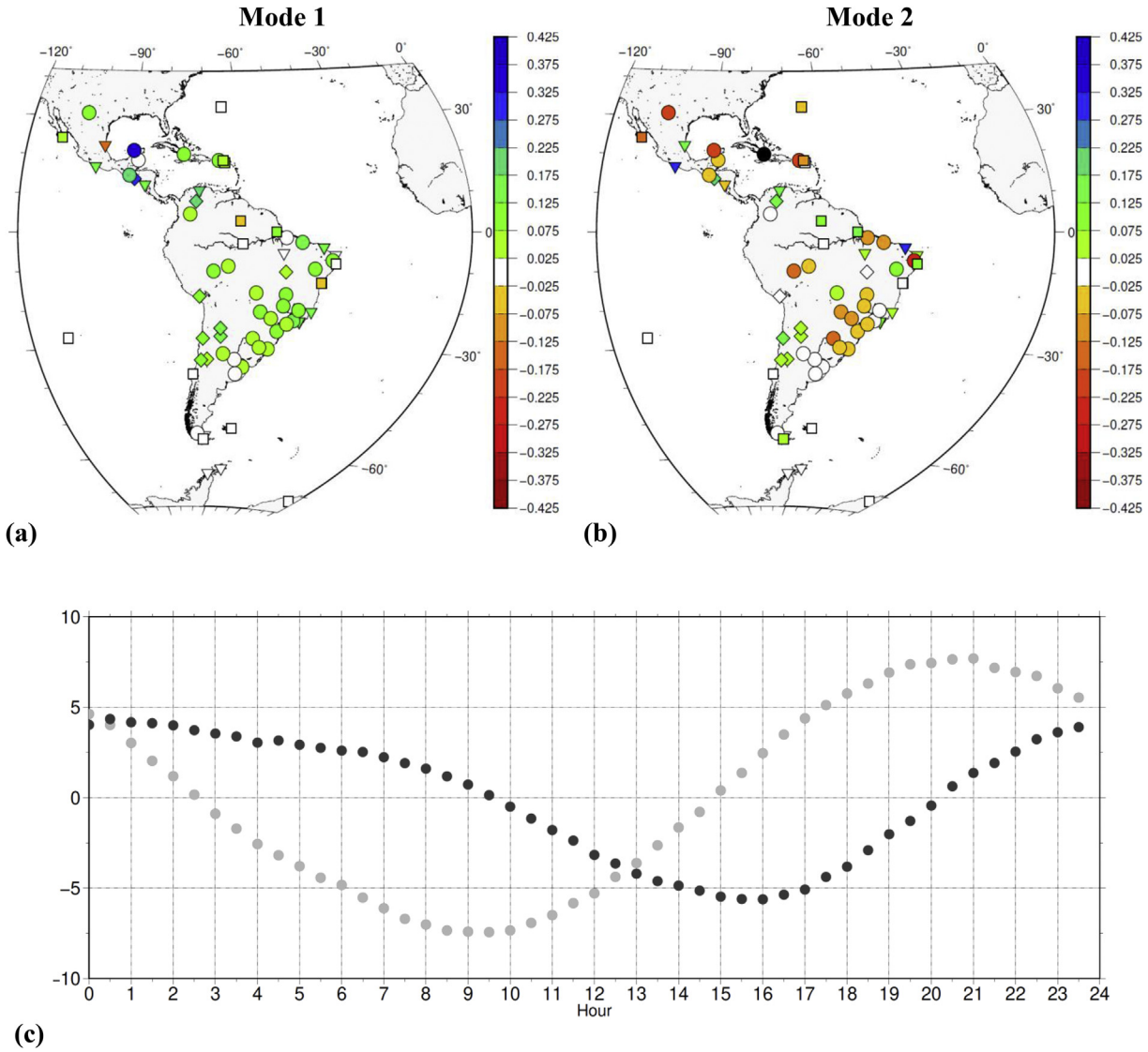

Fig. 9. PCA analysis for the JJA annual diurnal variability of PWV. (a) eigenvector of the first mode, $\boldsymbol{e_1}$; (b) eigenvector of the second mode,$\boldsymbol{e_2}$; (c) principal components of the first and second modes, a_1 (grey) and a_2 (black) respectively.

4. Discussions and conclusions

This work is focused on the study of the annual and seasonal diurnal variability of PWV over Central and South America. The performed analysis also included the surface temperature measurements (T). PCA was applied to the diurnal anomalies (differences between the values at each instant and the daily mean values) of each parameter, i.e. PWV and T. Therefore, the numerical technique is used to represent the main sub-daily variation where the first two modes represent more than 90% of the PWV variability.

The range of PWV values in the region under study is very wide. From areas in tropical climates with large PWV values (in particular of the climate subtype "tropical monsoon", with typical values near 54 kg/m^2) to areas in cold polar climates (with typical values of around 5 kg/m^2). Moreover, the distribution of PWV values also varies strongly with the temperature, being more evident for stations with desert climate, whose PWV values reach 40 kg/m^2 and 10 kg/m^2 for high and low temperature (see Fig. 3d), respectively. PWV values for temperate, polar and cold dry climate show a positive skewed distribution, whereas for tropical climates (except for monsoon) a negative skewed distribution is presented. Some researchers related these behaviors to the specific distributions functions. They found that the subtropical and temperate climates follow a lognormal distribution, and the tropical oceanic climate shows a reversed lognormal distribution. They also found a bimodal distribution in special cases (related with a distinct precipitable water modes) [27] and a Weisbull distribution was also found in temperate climate [28]. All of them highlight the strong dependence between the temperature and the pattern behavior of PWV.

From the analysis of the histograms for each GNSS station, it is found that the value of PWV is strongly related with the geographic latitude, being larger at lower latitudes. As expected, for stations located at similar latitudes, the value of PWV is larger at lower heights. The annual and seasonal PWV diurnal variation

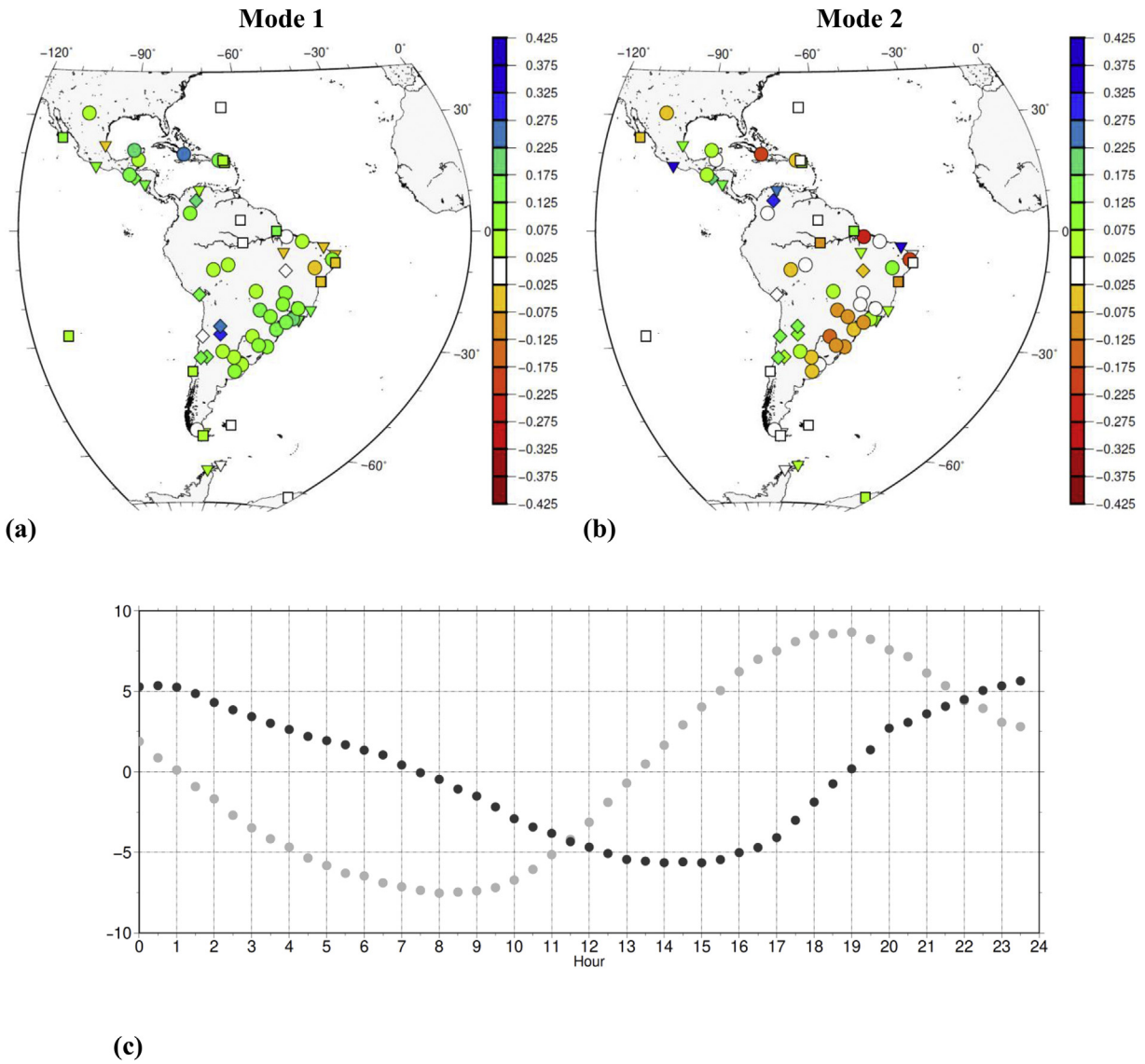

Fig. 10. PCA analysis for the SON annual diurnal variability of PWV. (a) eigenvector of the first mode, $\boldsymbol{e_1}$; (b) eigenvector of the second mode, $\boldsymbol{e_2}$; (c) principal components of the first and second modes, a_1 (grey) and a_2 (black) respectively.

was analyzed taking into account the topography of the station emplacement. At those stations classified as inland the temperature and the surface conditions (to yield evaporation) are the main agents producing the diurnal variability of PWV. The maximum value is recorded at least 2 h shifting to the maximum of temperature variability. In these cases, the PWV variability is mainly described by the first mode with positive eigenvector values. In some cases, the principal component of the second mode has an important contribution because it has negative values of the eigenvectors and the maximum PWV variability shifts to earlier hours. For stations classified as coastal and valley, the maximum of PWV variability is displaced to much later hours, between 23:00 LT and 1:00 LT. In these cases, the PWV variability is mainly described by the second mode with positive eigenvector values. A possible agent that causes the displacement of the maximum of the variability to the night hours is the effect of the sea/valley breeze. There are also stations that were classified as "undefined" surrounded by different bodies of water. Here we find that the maximum of PWV is previous or coincident to the maximum of variability in T. In these cases, the PWV variability is mainly described by the second mode with negative eigenvector values. One result of the previous PWV variability could be produced when the morning sea breeze is replaced by much dryer air if the wind changes direction. All inland stations and most of the coastal and valley stations located at mid-latitudes show the maximum amplitude of diurnal variability of PWV at the local summer. For those stations located at equatorial and low-latitude regions the maximum amplitude of diurnal variability of PWV is found during the equinoxes.

There are some stations where the behavior of diurnal variability of PWV has a marked seasonal effect. Some "valley" and "undefined" stations are representative of this behavior, highlighting the significance of the valley breeze during some seasons, and the influence of the temperature and the surface conditions (to

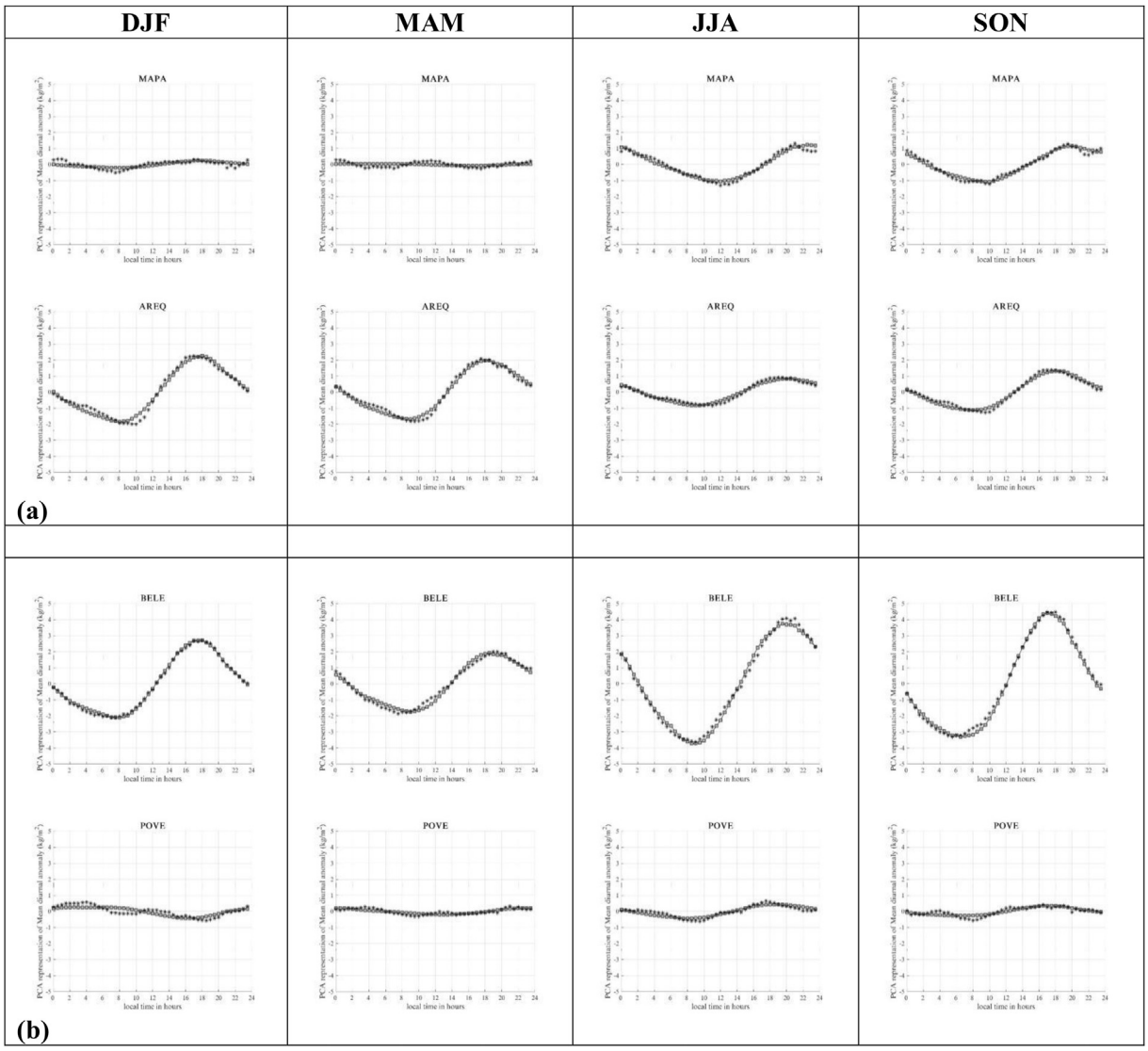

Fig. 11. Reconstruction of the seasonal diurnal variability of PWV using the first and the second PCA modes for selected stations (square) and the original cycle (asterisk).

yield evaporation) during the rest of the year. As well, two inland stations (BELE and POVE) show the effect of sea breeze just in one season of the year. One main possible reason could be that they are surrounded by a large river.

Conflicts of interest

The authors declare that there are no conflicts of interest.

Acknowledgments

This research was supported by the National Scientific and Technical Council of Argentina (CONICET) PIP 112-201201-00292, ANPCyT grant PICT 20121484 and Universidad Nacional de La Plata (UNLP) project 11G/142. We would like to thank the Department of Atmospheric Sciences of University of Wyoming for synoptic data used in this work.

References

[1] Jonathan Michael Hobbs, Characterizing Diurnal and Interannual Variability in the Atmosphere through Physical and Stochastic Models, Graduate Theses and Dissertations, 2014.
[2] K.E. Trenberth, Water Cycles and Climate Change. Global Environmental Change, Springer, Heidelberg, 2011.
[3] A. Dai, K.E. Trenberth, T.R. Karl, Effects of clouds, soil moisture, precipitation, and water vapor on diurnal temperature range, J. Clim. 12 (1999) 2451–2473, https://doi.org/10.1175/1520-0442(1999)012<2451:EOCSMP>2.0.CO;2.
[4] A. Dai, F. Giorgi, K.E. Trenberth, Observed and model-simulated diurnal cycles of precipitation over the contiguous United States, J. Geophys. Res. 104 (1999) 6377–6402, https://doi.org/10.1029/98JD02720.
[5] A. Dai, J. Wang, R.H. Ware, T. Van Hove, Diurnal variation in water vapor over North America and its implications for sampling errors in radiosonde humidity, J. Geophys. Res. 107 (2002), https://doi.org/10.1029/2001JD000642.
[6] M. Bevis, S. Businger, T.A. Herring, C. Rocken, R.A. Anthes, R.H. Ware, GPS meteorology: remote sensing of atmospheric water vapor using the global positioning system, J. Geophys. Res. Atmos. 97 (1992) 15787–15801, https://doi.org/10.1029/92JD01517.
[7] M. Bevis, S. Businger, S. Chiswell, T.A. Herring, R.A. Anthes, C. Rocken, R.H. Ware, GPS meteorology: mapping zenith wet delays onto precipitable water, J. Appl. Meteorol. 33 (1994) 379–386, https://doi.org/10.1175/1520-0450(1994)033<0379:GMMZWD>2.0.CO;2.

[8] J. Duan, M. Bevis, P. Fang, Y. Bock, S. Chiswell, S. Businger, C. Rocken, F. Solheim, T. van Hove, R. Ware, S. McClusky, T.A. Herring, R.W. King, GPS meteorology: direct estimation of the absolute value of precipitable water, J. Appl. Meteorol. 35 (1996) 830–838, https://doi.org/10.1175/1520-0450(1996)035<0830:GMDEOT>2.0.CO;2.
[9] C. Bianchi, L. Mendoza, L.I. Fernández, M.P. Natali, A. Meza, J.F. Moirano, Multi-year GNSS monitoring of atmospheric IWV over Central and South America for climate studies, Ann. Geophys. 34 (2016) 623–639, https://doi.org/10.5194/angeo-34-623-2016.
[10] G. Guerova, J.-M. Bettems, E. Brockmann, C. Matzler, Assimilation of the GPS-derived integrated water vapour (IWV) in the Meteo Swiss numerical weather prediction model - a first experiment, Phys. Chem. Earth 29 (2004) 177–186.
[11] R.H. Ware, D.W. Fulker, S.A. Stein, D.N. Anderson, S.K. Avery, R.D.C.K.K. Droegemeier, J.P. Kuettner, J. Minster, S. Sorooshian, Real-time national GPS networks: opportunities for atmospheric sensing, Earth Planets Space 52 (2000) 901–905.
[12] G. Gendt, C. Reigber, G. Dick, Near real-time water vapor estimation in a German GPS network - results from the ground program of HGF GASP project, Phys. Chem. Earth Part A 26 (2001) 413–416, https://doi.org/10.1016/S1464-1895(01)00075-8.
[13] C. Rocken, J. Braun, T. Van Hove, J. Johnson, Y.-H. Kuo, Developments in Ground-Based GPS meteorology,Proceedings, International Workshop on GPS Meteorology, Tsukuba, Japan, 2003, pp. 1–6.
[14] B. Radhakrishna, F. Fabry, J.J. Braun, T. Van Hove, Precipitable water from GPS over the continental United States: diurnal cycle, intercomparisons with NARR, and link with convective initiation, J. Clim. 28 (2015) 2584–2599, https://doi.org/10.1175/JCLI-D-14-00366.1.
[15] J.P. Ortiz de Galisteo, V. Cachorro, C. Toledano, B. Torres, N. Laulainen, Y. Bennouna, A. de Frutos, Diurnal cycle of precipitable water vapor over Spain, Q. J. R. Meteorol. Soc. 137 (2011) 948–995, https://doi.org/10.1002/qj.811.
[16] E. Jakobson, H. Keernik, A. Luhamaa, H. Ohvril, Diurnal variability of waper vapour in the Baltic Sea region according to NCEP_CFSR and BaltAn65+ reanalyses, Oceanologia 56 (2) (2014) 191–204. https://doi:10.5697/oc.56-2.191.
[17] V.V. Kalinnikov, O.G. Khutorova, Diurnal variations in integrated water vapor derived from a GPS ground network in the Volga–Ural region of Russia, Ann. Geophys. 35 (2017) 453–464, https://doi.org/10.5194/angeo-35-453-2017.
[18] G. Li, F. Kimura, T. Sato, D. Huang, A composite analysis of diurnal cycle of GPS precipitable water vapor in central Japan during Calm Summer Days, Theor. Appl. Climatol. 92 (2008) 15–29, https://doi.org/10.1007/s00704-006-0293-x.
[19] J.D. Neelin, O. Peters, K. Hales, The transition to strong convection, J. Atmos. Sci. 66 (2009) 2367–2384, https://doi.org/10.1175/2009JAS2962.1.
[20] C.S. Bretherton, J.R. McCaa, H. Grenier, A new parameterization for shallow cumulus convection and its application to marine subtropical cloud-topped boundary layers. Part I: description and 1D results, Mon. Weather Rev. 132 (2004) 864–882, https://doi.org/10.1175/1520-0493(2004)132<0864:ANPFSC>2.0.CO;2.
[21] D.K. Adams, R.M. Fernandes, K.L. Holub, S.I. Gutman, H.M. Barbosa, L.A. Machado, A.J. Calheiros, R.A. Bennett, E.R. Kursinski, L.F. Sapucci, C. DeMets, G.F. Chagas, A. Arellano, N. Filizola, A.A. Amorim Rocha, R.A. Silva, L.M. Assunção, G.G. Cirino, T. Pauliquevis, B.T. Portela, A. Sá, J.M. de Sousa, L.M. Tanaka, The Amazon dense GNSS meteorological network: a new approach for examining water vapor and deep convection interactions in the Tropics, Bull. Am. Meteorol. Soc. 96 (2015) 2151–2165, https://doi.org/10.1175/BAMS-D-13-00171.1.
[22] R.W. Preisendorfer, Principal Component Analysis in Meteorology and Oceanography, Elsevier, Amsterdam, 1988.
[23] H. Wackernagel, Multivariate Geostatistics: An Introduction with Applications, second ed., Springer-Verlag, Berlin Heidelberg, 1998.
[24] M.C. Peel, B.L. Finlayson, T.A. McMahon, Updated world map of the Köppen-Geiger climate classification, Hydrol. Earth Syst. Sci. 11 (2007) 1633–1644, https://doi.org/10.5194/hess-11-1633.
[25] M. Kottek, J. Grieser, C. Beck, B. Rudolf, F. Rubel, World Map of the Köppen-Geiger climate classification updated, Meteorol. Z. 15 (2006) 259–263, https://doi.org/10.1127/0941-2948/2006/0130.
[26] H. Diedrich, F. Wittchen, R. Preusker, J. Fischer, Representativeness of total column water vapour retrievals from instruments on polar orbiting satellites, Atmos. Chem. Phys. 16 (2016) 8331–8339, https://doi.org/10.5194/acp-16-8331-2016.
[27] J. Foster, M. Bevis, W. Raymond, Precipitable water and the lognormal distribution, J. Geophys. Res. 111 (2006) D15102, https://doi.org/10.1029/2005JD006731.
[28] A. Iassamen, H. Sauvageot, N. Jeannin, S. Ameur, Distribution of tropospheric water vapor in clear and cloudy conditions from microwave radiometric profiling, J. Appl. Meteorol. Climatol. 48 (2009) 600–615, https://doi.org/10.1175/2008JAMC1916.1.

Amalia Meza: Associate Professor at University, Universidad Nacional de La Plata. PhD in Astronomy. Permanent position as full time researcher at CONICET (Argentinean Research Council), since 2002. Head of MAGGIA (Meteorología espacial, Atmósfera terrestre, Geodesia,Geodinámica, diseño de Instrumental y Astrometría)laboratory, which belong to University of La Plata (UNLP). More than 25 years of experience in Satellite Geodesy and Aeronomy. Main topics of interest: atmosphere modeling from GNSS data, physical correlation with water vapor and total electron content variability and tropospheric /ionosphere effects on geodetic positioning.

Luciano P. O. Mendoza: was born in Buenos Aires (Argentina) in April 1976. He graduated in Astronomy at the Universidad Nacional de La Plata (UNLP, Argentina) in 2005, and completed his PhD work at the same university in 2008, including a one-year scholarship at the Technische Universität Dresden (TUD, Germany). He currently holds a full-time research position at the Comisión Nacional de Investigaciones Científicas y Técnicas (CONICET, Argentina), working at the Laboratorio de Meteorología espacial, Atmósfera terrestre, Geodesia, Geodinámica, diseño de Instrumental y Astrometría (MAGGIA, UNLP). His main field of work has been research and monitoring in Geodynamics, Geodesy and, more recently, Atmospheric Sciences. He led the development of an innovative system for monitoring the ionosphere in South America, in almost real time and using multi-GNSS data, and directed several projects for the study of geodynamic processes in Southern Patagonia.

María Paula Natali: teaching assistant Professor at Universidad Nacional de La Plata. PhD in Astronomy. Permanent position as full time researcher at CONICET (Argentinean Research Council), since 2010. Member of MAGGIA (Meteorología espacial, Atmósfera terrestre, Geodesia,Geodinámica, diseño de Instrumental y Astrometría)laboratory, which belong to University of La Plata (UNLP). More than 20 years of experience in Satellite Geodesy and Aeronomy. Main topics of interest: Application of the GNSS systems for the estimation of integrated water vapour (IWV) and the Total Electron Content (TEC) in the atmosphere.

Clara Bianchi: Head Teaching Assistant (HTA), Universidad Nacional de La Plata. PhD in Astronomy. Main topics of interest: satellite geodesy, GNSS Meteorology, and GNSS natural hazards monitoring.

Laura Fernández: Associate Professor at University, Universidad Nacional de La Plata. PhD in Astronomy. Permanent position as full time researcher at CONICET (Argentinean Research Council). Member of MAGGIA (Meteorología espacial, Atmósfera terrestre, Geodesia,Geodinámica, diseño de Instrumental y Astrometría) laboratory, which belong to University of La Plata (UNLP). Main topics of interest: regional analysis of the atmospheric water vapor from GNSS. Earth rotation.